

# SCIENTIFIC REPORTS



OPEN

## A Critical, Nonlinear Threshold Dictates Bacterial Invasion and Initial Kinetics During Influenza

Amber M. Smith & Amanda P. Smith

Received: 23 May 2016

Accepted: 18 October 2016

Published: 15 December 2016

Secondary bacterial infections increase morbidity and mortality of influenza A virus (IAV) infections. Bacteria are able to invade due to virus-induced depletion of alveolar macrophages (AMs), but this is not the only contributing factor. By analyzing a kinetic model, we uncovered a nonlinear initial dose threshold that is dependent on the amount of virus-induced AM depletion. The threshold separates the growth and clearance phenotypes such that bacteria decline for dose-AM depletion combinations below the threshold, stay constant near the threshold, and increase above the threshold. In addition, the distance from the threshold correlates to the growth rate. Because AM depletion changes throughout an IAV infection, the dose requirement for bacterial invasion also changes accordingly. Using the threshold, we found that the dose requirement drops dramatically during the first 7d of IAV infection. We then validated these analytical predictions by infecting mice with doses below or above the predicted threshold over the course of IAV infection. These results identify the nonlinear way in which two independent factors work together to support successful post-influenza bacterial invasion. They provide insight into coinfection timing, the heterogeneity in outcome, the probability of acquiring a coinfection, and the use of new therapeutic strategies to combat viral-bacterial coinfections.

Influenza A virus (IAV) poses a considerable threat to public health, resulting in 15–65 million infections and >200,000 hospitalizations each year during seasonal epidemics in the U.S.<sup>1,2</sup>. Morbidity and mortality increase when a pandemic strain emerges and/or when IAV infection is complicated by a bacterial pathogen like *Streptococcus pneumoniae* (pneumococcus), which has accounted for 40–95% of influenza-related mortality in past pandemics<sup>3–6</sup>. As the respiratory tract environment deteriorates during influenza, the physiological barriers and immune mechanisms that normally clear pathogens become compromised and bacteria are able to invade and grow rapidly. Several factors, including viral and bacterial strain, inoculum size, and bacterial infection timing, are thought to contribute to influenza-bacterial coinfection kinetics, pathogenicity, and the likelihood of severe pneumonia developing (reviewed in refs 7, 8, 9, 10, 11, 12 and 13). Understanding how each factor influences the virulence and interaction between influenza viruses and bacterial pathogens and how each is interrelated is pivotal to finding effective preventative and therapeutic strategies.

Although well-characterized animal models have allowed for the study of various factors that affect bacterial acquisition and pathogenicity after influenza (reviewed in ref. 11), the extraordinary complexity of host-pathogen and pathogen-pathogen interplay complicates investigating every possible interaction simultaneously. Quantitative analyses have made it possible to simultaneously assess the contributions of different components and identify critical mechanisms driving influenza-bacterial coinfection kinetics. We recently combined a mathematical model and data from animal studies to establish dynamical host-pathogen feedbacks, quantify the contribution of various hypothesized mechanisms (e.g., virus enhanced bacterial attachment<sup>14,15</sup> and alveolar macrophage (AM) inhibition<sup>16</sup>), and develop new hypotheses (i.e., bacteria enhanced virus production) about the relationship between influenza and pneumococcus<sup>17</sup>. Our mathematical model revealed that the rapid increase in bacterial loads, a hallmark of influenza-pneumococcal coinfection, is initiated by the virus removing the protective effect of alveolar macrophages (AMs) with 85–90% efficiency by 7d post-influenza infection (pii) and that bacterial clearance could be achieved with improved AM response. This was in correlation to one experimental study suggesting that the phagocytic ability of these cells is inhibited<sup>16</sup>. It was initially unclear from either study if the effect accumulates over time and if it comprises several underlying mechanisms. However, a more recent experimental study followed up these works by using an advanced gating strategy to better define the AM

Department of Infectious Diseases, St. Jude Children's Research Hospital, Memphis, TN 38105, USA. Correspondence and requests for materials should be addressed to A.M.S. (email: amber.smith@stjude.org)

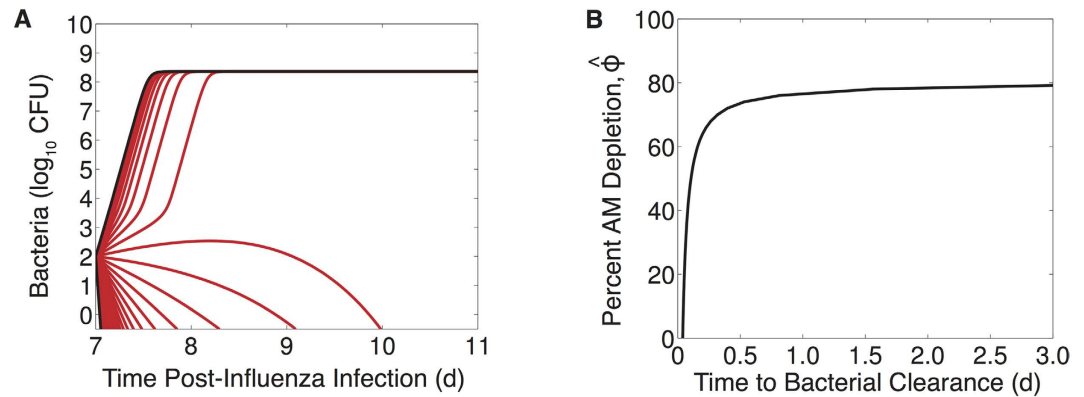


**Figure 1. Simulation of the coinfection model for various levels of AM depletion.** (A) Simulation of the coinfection model (Equations (2–6)) using the parameter values in Table S1 that were optimized for an infection with  $10^2$  TCID<sub>50</sub> PR8 followed 7d later by  $10^3$  CFU D39 and values of AM depletion ( $\phi$ ) ranging from no impairment ( $\phi = 0$ ), which results in immediate clearance, to 100% impairment ( $\phi = 1$ ), which results in immediate growth to the maximum carrying capacity. (B) The number of days until complete bacterial clearance ( $\log_{10}P(t) < 0$ , where  $P(t)$  is the solution to Equation (6)) occurs for AM depletion between 0% and 100%.

population throughout the course of an IAV infection and found that these cells are depleted<sup>18</sup>, rather than or in addition to their functional inhibition, by IAV and that the level of depletion corresponds to the amount of bacterial outgrowth<sup>18</sup>. While our mathematical model does not distinguish between these mechanisms, the AM data indicated that the maximum amount of depletion occurred 7d p.i. and matched our parameter estimate of 85–90%<sup>18</sup>. Further, our model did include a handling time effect on the rate of bacterial phagocytosis by AMs, which had only a minor role. This further supports AM depletion as the dominant mechanism driving bacterial establishment, with functional inhibition as a possible secondary mechanism, and the accuracy of our model. Remarkably, this also corresponds to the time when bacterial coinfections are the most lethal<sup>19</sup>. The underlying mechanism resulting in the loss of AMs during influenza virus infection is currently unknown.

Another important feature of influenza-pneumococcal coinfection biology is that bacteria grow rapidly for initial doses that would be rapidly cleared in the absence of virus<sup>17,19</sup>. In both naive and influenza-infected hosts, the trajectory of bacterial titers is dependent on the inoculating dose<sup>16,17,20–22</sup>. Further, in the context of the coinfection, a distinct dichotomous pattern emerged with a low dose ( $10^2$  CFU) compared to a higher dose ( $10^3$  CFU) such that some individuals had high bacterial titers, an indication of severe pneumonia, while others had low bacterial titers and, presumably, a more mild infection<sup>17</sup>. It is currently unclear what factors contribute to the differential dynamics, although we hypothesized that this may be due to heterogeneity in the AM population because reducing the depletion parameter in our mathematical model could result in lower titers<sup>17</sup> and because we previously related the dose dependent effect to the AM population in a naive host<sup>20</sup>. However, the exact connection between dose and AM depletion during influenza-pneumococcal coinfection is unclear. Understanding this behavior in more detail will help elucidate what conditions lead to secondary pneumococcal infections after influenza and why only a proportion of IAV infections lead to severe bacterial pneumonia<sup>23–26</sup>.

Here, we analyzed our coinfection model in more detail to quantify how the trajectory of bacterial growth changes with the level of AM depletion. In doing so, we uncovered a nonlinear initial dose threshold that is dependent on the number of AMs and found the critical number of AMs required to support a clearance phenotype. We then used this threshold together with data on the AM population<sup>18</sup> to predict how the dose requirement declines over the course of an IAV infection. To validate the time-dependent threshold predictions, we examine bacterial growth/clearance rates in groups of BALB/cJ mice infected with influenza A virus A/Puerto Rico/8/34 (H1N1) (PR8) then 1, 3, 5, 7, 9, or 11 days later with pneumococcal strain D39 at a dose larger or smaller than the predicted threshold. The resulting data agree with our theoretical predictions and, in doing so, define an important, nonlinear relationship between bacterial dose and AM depletion that can be used as a predictive tool. Taken together, our data gives new insight into the timing of coinfections, potential therapeutic strategies, and why bacterial coinfections occur more often during influenza pandemics compared to seasonal epidemics.

## Results

**Coinfection Kinetics Depend on AM Depletion.** To examine how pneumococcal kinetics during IAV infection change with varying degrees of AM depletion, we simulated the coinfection model (Equations (2–6)) with values of AM depletion ( $\phi$ ) ranging between 0% and 100% ( $0 \leq \phi \leq 1$ ). The resulting dynamics (Fig. 1A) illustrate that distinct bacterial outcomes (i.e., maximum growth or clearance) exist depending on the degree that the IAV infection reduces the AM population. Bacterial resolution is predicted to occur with minor AM depletion (small  $\phi$ ), but the length of time for bacterial loads to completely clear ( $\log_{10}P(t) < 0$ , where  $P(t)$  denotes the solution to Equation (6)) increases rapidly as depletion accumulates (increasing  $\phi$ ) and saturates once these cells have declined by ~80% (Fig. 1B).

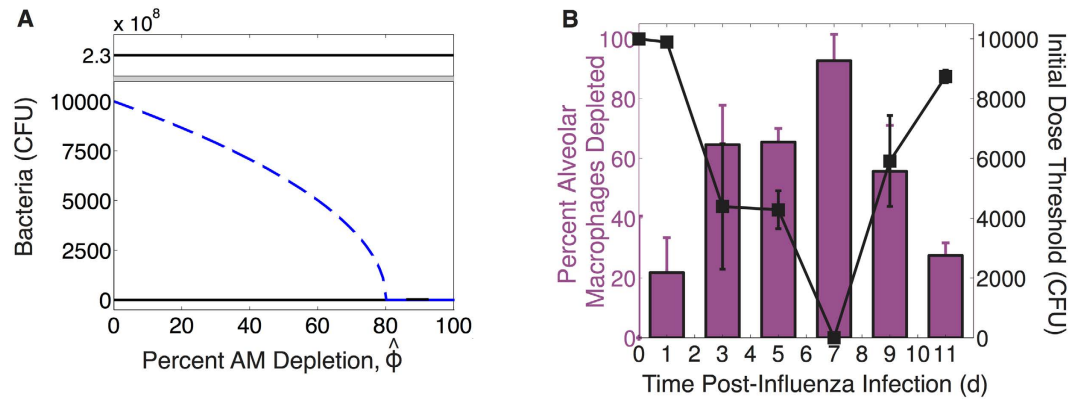


**Figure 2. Initial dose threshold dependence on AM depletion.** (A) Bacterial outcomes (steady states) for the coinfection model for different values of AM depletion ( $\phi$ ). Two possible outcomes exist, clearance (0 CFU) or growth to maximum carrying capacity ( $K_p = 2.3 \times 10^8$  CFU), and are indicated by solid black lines. The intermediate state (dashed blue line, defined by Equations (7)–(8)) is the initial dose threshold that dictates if bacterial loads will decline (doses below the threshold) or if they will increase (doses above the threshold). (B) The predicted threshold (black line, calculation in Table 1) over the course of an IAV infection given the amount of AM depletion<sup>18</sup>, Copyright 2013. The American Association of Immunologists, Inc. (magenta bars; see Methods).

**Initial Dose Threshold.** Because different levels of AM depletion result in different outcomes, we analyzed our coinfection model using mathematical steady-state and bifurcation analyses (see Methods). This analysis verified the two potential outcomes (stable steady states) as clearance ( $P = 0$  CFU) and sustained growth to maximum carrying capacity ( $P = K_p = 2.3 \times 10^8$  CFU) (Fig. 2A). An intermediate, unstable state given by Equations (7)–(8) is dependent on the extent of AM depletion and governs which of these outcomes manifests. This state predicts an initial dose threshold (Fig. 2A) such that bacteria will exhibit a growth phenotype for doses above the threshold and a clearance phenotype for doses below the threshold for a given amount of AM depletion. Further, the rate at which bacteria grow or clear will increase as the distance from the threshold increases. As AMs become more depleted, the dose needed to elicit an infection drops rapidly in a nonlinear manner. Once AMs are reduced by ~80%, as indicated by the near zero value of the threshold, any dose will support bacterial growth. This critical level of depletion ( $\hat{\phi}_{crit}$ ) can be analytically calculated (see the Supplementary Information) in terms of the model parameters (Table S1) as

$$\hat{\phi}_{crit} = 1 - \frac{\text{bacterial growth rate}}{\text{bacterial clearance rate by AMs}} = 1 - \frac{r}{\gamma_{M_A} M_A} = 79.98\%. \quad (1)$$

**Threshold Dynamics During IAV Infection.** Because AM depletion is dynamic during IAV infection<sup>18</sup> and the initial dose threshold is dependent on AM depletion, the initial dose threshold will change throughout the course of an IAV infection. To determine how the threshold changes with time, we used *in vivo* data on the number of AMs lost at 1, 3, 5, 9, and 11 d pii (see Methods) (Fig. 2B) as an approximation for the parameter  $\phi$  in Equation (6) because our estimated parameter value<sup>17</sup> matched the empirical value<sup>18</sup> for a coinfection at 7 d pii. We used the mean and the standard deviation of the AM data to obtain an estimated confidence interval for  $\phi$  for each time point (Table 1). We then used these values together with the model solution for virus ( $V(t)$ ) at each time point to calculate the overall effect of depletion, defined by  $\hat{\phi} = \phi V / (K_{PV} + V)$  in Equation (6), and the corresponding initial dose threshold value at each coinfection time (Table 1). The resulting threshold drops rapidly between 1 d and 3 d pii, reducing the dose necessary for a secondary infection to establish by over 50% (Fig. 2B). The threshold decreases by another 50% by 7 d pii before increasing to near baseline level at 11 d pii.

**Bacterial Growth for Doses Below or Above the Threshold.** The initial dose threshold indicates that bacteria will clear for doses lower than the threshold and grow for doses higher than the threshold. To test the predicted dynamic threshold, we infected groups of mice first with 50 TCID<sub>50</sub> PR8 then D39 at 1, 3, 5, 7, 9, or 11 d pii at a bacterial dose below or above the predicted threshold value (Table 2). For bacterial infection at 7 d pii, a dose below the threshold was not examined due to the predicted value being less than 1 CFU. We then quantified bacterial growth at 4 h and 24 h post-bacterial infection (pbi).

When inoculating with a dose below the predicted threshold, we found that bacterial loads at 4 h pbi were significantly lower ( $p < 0.05$ ) than the inoculum in all mice for all coinfection times tested (Fig. 3A). This initial clearance supports our predicted threshold, which suggests that doses below the threshold will result in bacterial clearance. For a coinfection at 1 d pii or 3 d pii and for the doses used, bacteria were undetectable in 2 out of 5 mice. To investigate whether clearance could also be attained with a dose closer to the threshold value, we inoculated a group of influenza-infected mice with  $7.55 \times 10^3$  CFU (compared to  $3.55 \times 10^3$  CFU) D39 at 1 d pii. At this dose, bacterial loads decreased in all mice ( $p < 0.05$ ) but none resolved the infection within 4 h pbi (data not shown). Conversely, we also examined a dose lower than the low dose in Table 2 ( $1 \times 10^3$  CFU compared to  $2.7 \times 10^3$  CFU) for bacterial infection 5 d pii and found that the rate of clearance improved and that 1 out of 5 mice resolved the infection ( $p < 0.05$ ) (Fig. 4B).

Coinfection Day	Percent AM Depletion Estimate of $\phi$	Virus, $\log_{10} V(t)$ Model Solution <sup>17</sup> ( $\log_{10} \text{TCID}_{50}$ )	Percent Overall AM Depletion $\hat{\phi} = \phi \frac{V(t)}{K_{PV} + V(t)}$	Initial Dose Threshold Equations (7–8), $\times 10^3$ (CFU)
1	21.8 [10.2, 33.5]	2.2	1.9 [0.02, 19.5]	9.89 [9.83, 9.94]
3	64.6 [51.4, 77.8]	6.7	64.6 [50.9, 77.8]	4.39 [2.29, 6.49]
5	65.4 [60.9, 70.0]	6.1	65.3 [58.7, 70.0]	4.28 [3.65, 4.91]
7	92.7 [83.9, 100]	5.3	91.8 [43.2, 100]	$2.2 \times 10^{-5}$ [ $4.3 \times 10^{-6}$ , $5.2 \times 10^{-5}$ ]
9	55.7 [40.3, 71.1]	4.5	52.9 [0.67, 71.1]	5.91 [4.39, 7.43]
11	27.5 [23.3, 31.7]	3.7	20.9 [0.05, 31.7]	8.74 [8.54, 8.94]

**Table 1. Calculation of the estimated initial dose threshold.** The threshold (Equations (7–8)) is calculated using the overall AM depletion estimate ( $\hat{\phi} = \phi V(t)/(K_{PV} + V(t))$ ), where  $\phi$  is estimated by the percent AM depletion<sup>18</sup> (Copyright 2013. The American Association of Immunologists, Inc.; Fig. 2B) and  $V(t)$  is the coinfection model solution for virus.

Coinfection Day	Threshold $\times 10^3$ (CFU)	Dose Below Threshold $\times 10^3$ (CFU)	Dose Above Threshold $\times 10^3$ (CFU)
1	9.89	3.50	10.7
3	4.39	2.75	9.40
5	4.28	2.70	5.90
7	$2.2 \times 10^{-5}$	—	0.50
9	5.91	3.90	8.90
11	8.74	3.65	10.0

**Table 2. Bacterial doses used to test the predicted initial dose threshold.**

We next examined bacterial titers at 24 h pbi in a separate group of mice using the low doses in Table 2 to determine if titers would continue to decline. For coinfection at 1d and 3d pii, where 40% had resolved the infection within 4 h, the same proportion of individuals had undetectable titers at 24 h pbi. If bacteria were not controlled within this time frame, then the initial clearance mechanisms were overcome and bacterial loads surpassed those at 4 h and, in some cases, the inoculum (Fig. 3A). The average rate of growth between 4 h and 24 h inversely correlated to the average clearance rate between 0 h and 4 h such that slower clearance supported faster growth (Fig. 3B) and less titer heterogeneity (Fig. 3A).

When mice were given a dose slightly above the threshold, bacterial loads at 4 h pbi remained relatively constant ( $p > 0.05$ ) for all coinfection timings with 50–60% of individuals partially cleared the inoculum and the remaining 40–50% showed rapid growth (Fig. 4A). To find the dose where 100% of infections result in immediate growth and to show that growth increases with the distance from the threshold, we infected groups of mice at 5d pii with doses incrementally higher than in Table 2 (7.0, 8.5, or  $10.5 \times 10^3$  CFU) (Fig. 4B,C). At  $7 \times 10^3$  CFU, some individuals were still able to partially clear the inoculum ( $p > 0.05$ ). However, at  $8.5 \times 10^3$  CFU and  $10.5 \times 10^3$  CFU, bacteria readily grew in all individuals to levels higher than the inoculum ( $p < 0.005$ ). In addition, the strength of this growth increased and the titer heterogeneity decreased as the dose increased (Fig. 4C,D).

To examine bacterial growth when AMs are depleted by a source other than virus, we gave naive mice clodronate-liposomes, which effectively reduced the AM population in the lung through cell death<sup>27</sup>. At 4 h post-clodronate (pc), the AM population was reduced by ~75–80% (Fig. 5A). Because this value is close to the critical level of AMs (Equation (1)), we infected groups of mice at 4 h pc with either 1 CFU, 10 CFU, or 100 CFU D39. At 1 CFU, we detected bacteria in 1/5 mice at 4 h pbi. At 10 CFU and 100 CFU, bacterial loads were higher than the inoculum in all 5 mice ( $p > 0.05$  and  $p < 0.005$ , respectively) (Fig. 5B).

## Discussion

Secondary bacterial infections increase the severity of influenza-associated illnesses and the mortality rates during influenza pandemics<sup>3–6</sup>. However, not every IAV infection results in a bacterial invasion and only a proportion of successful coinfections lead to severe pneumonia<sup>23,24</sup>. The probability of pneumonia manifesting during influenza is multifactorial and may involve several pathogen and host characteristics, including viral and bacterial strain, dose, and host immune status (reviewed in refs 7, 8, 9, 10, 11, 12, 13). Identifying which factors promote coinfection, how each affects the kinetics, the pathogenicity, and the likelihood of bacterial pneumonia following influenza, and how they are interrelated could identify new targets for treating or preventing secondary infections.

Our analyses and experiments pinpointed the way in which bacterial dynamics vary depending on the bacterial dose and the AM population size, and identified the combinations of these two factors that lead to distinct phenotypes. In particular, we showed that an early clearance phenotype exists for doses below an initial dose threshold, a growth phenotype for doses sufficiently above the threshold, and a dichotomous phenotype for doses close to the threshold (Figs 3, 4 and 5). We also show that the relationship between bacterial dose and the level of AM depletion is independent of what causes the reduction in AMs (e.g., virus infection via an unknown mechanism (Figs 3 and 4) or clodronate-liposomes via cell death (Fig. 5)) and that 1–10 CFU is sufficient to yield bacterial growth when the depletion is ~80% (Fig. 5B). The nonlinearity of the relationship between dose

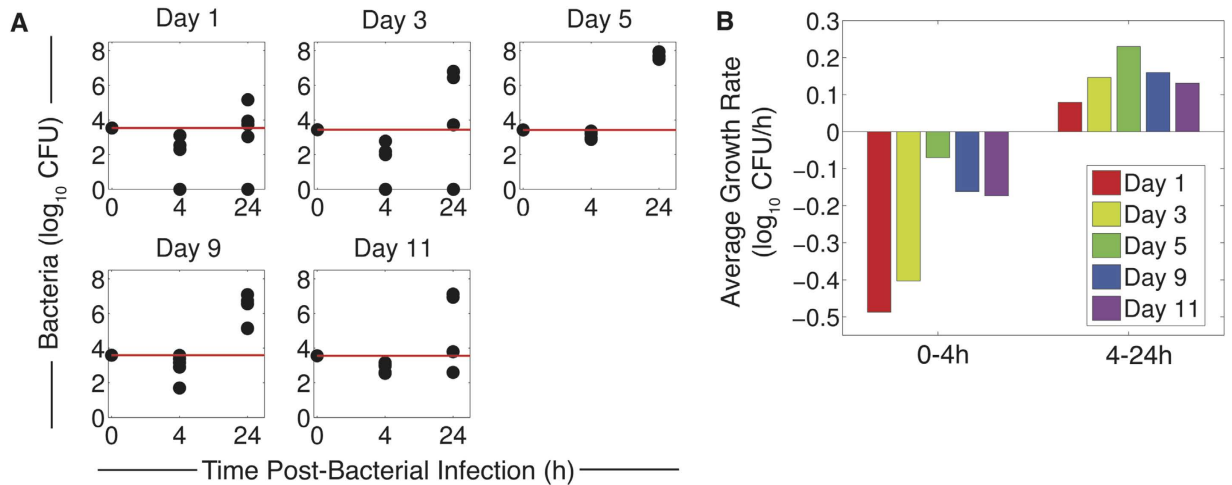


**Figure 3. Bacterial growth for doses below the threshold.** (A) Bacterial loads ( $\log_{10}$  CFU) at 4 h and 24 h pbi for PR8 infection followed by D39 at the indicated coinfection time (1, 3, 5, 9, or 11 d pii) at doses below the threshold (Table 2). The red line indicates the inoculum size and each dot represents an individual mouse (5 mice/group). (B) Average  $\log_{10}$  rate of bacterial growth from 0 h to 4 h pbi and from 4 h to 24 h pbi for coinfection at 1, 3, 5, 9 or 11 d pii at the indicated coinfection time.

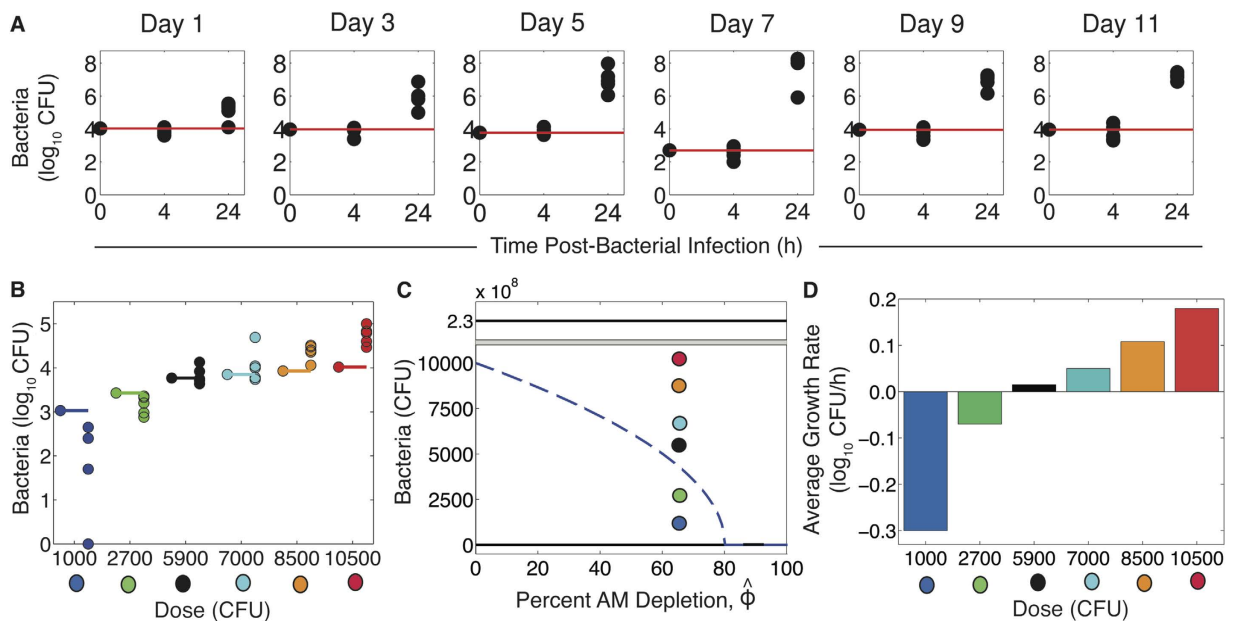


**Figure 4. Bacterial growth for doses above the threshold.** (A) Bacterial loads ( $\log_{10}$  CFU) at 4 h and 24 h pbi for PR8 infection followed by D39 at the indicated coinfection time (1, 3, 5, 7, 9, or 11 d pii) at doses above the threshold (Table 2). (B) Bacterial loads ( $\log_{10}$  CFU) at 4 h pbi for PR8 infection followed by D39 at 5 d pii at the indicated dose (single dots on the left) with (C) the corresponding location relative to the threshold and (D) the average  $\log_{10}$  bacterial growth rate from 0 h to 4 h pbi. Colored lines indicate the inoculum size and each dot represents an individual mouse (5 mice/group).

and AM depletion is important and non-intuitive, even with our previous knowledge that these two effects are related<sup>16,20–22</sup> and that they both influence coinfection kinetics<sup>16–19</sup>. Knowing how the combination of two factors work together and quantifying the conditions that yield each of the outcomes in addition to the trajectory of bacterial titers is crucial to understanding coinfection kinetics. It also allows us to predict the conditions given the behavior and vice versa.

For example, we observed that initial bacterial clearance yields larger heterogeneity in bacterial loads as the infection progresses (Figs 3A and 4A). This knowledge has given us insight into the dynamics observed in other datasets that were previously unexplained. We noted two datasets in our earlier work<sup>17</sup> where bacterial titers split into two groups such that ~50% were at high levels and ~50% were at low levels (Figure S3). In the first dataset (Figure S3A), groups of mice were infected with the same virus (PR8) but with different bacterial doses ( $10^2$  or

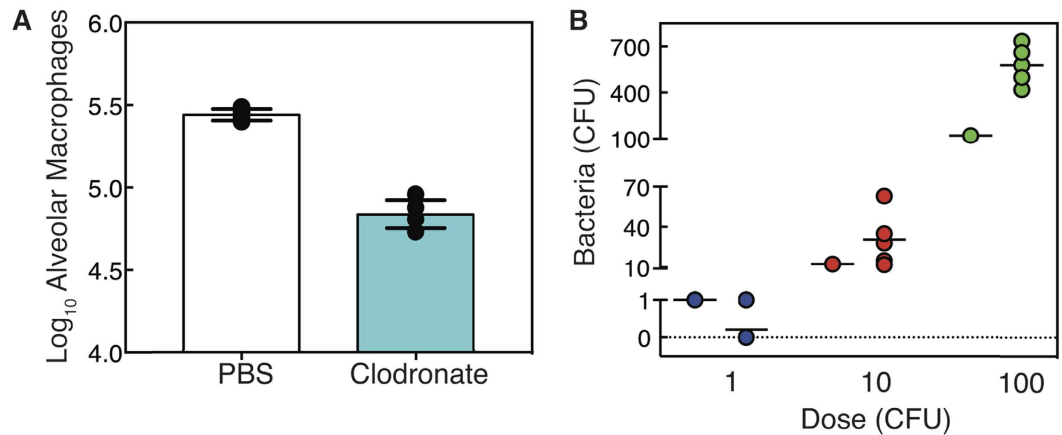


**Figure 5. Bacterial growth after depletion of AMs by clodronate-liposome induced cell death.** (A) Absolute number of AMs at 4 h for mice given either PBS (white) or clodronate-liposomes (cyan). Bars are the average values, lines are the standard deviation, and each dot represents an individual mouse (5 mice/group). (B) Bacterial growth (CFU) at 4 h pbi for mice given clodronate-liposomes and infected with D39 at 4 h pc at the indicated dose. Black lines are the average value, single dots on the left indicate the inoculum size, and each dot represents an individual mouse (5 mice/group).

$10^3$  CFU) 7d pii<sup>17</sup>. For the larger dose ( $10^3$  CFU), little heterogeneity was observed in the data and bacterial growth at 4 h pbi was at or above the inoculum (Figure S2B). This is consistent with a dose that is above the threshold. Comparatively, the lower dose ( $10^2$  CFU) resulted in some mice with high titers and some mice with low titers, which indicates a dose that is close to or below the threshold (Figure S3A). In the second dataset (Figure S3B), mice were infected with different viruses (PR8 or PR8-PB1-F2(1918)) and the same bacterial dose ( $10^3$  CFU) 7d pii<sup>17</sup>. Bacterial titers for a coinfection with the PR8-PB1-F2(1918) virus split into two groups (Figure S3B), which is consistent with an AM:dose ratio closer to the threshold, whereas little heterogeneity was observed for coinfection with the PR8 virus (Figure S2B). We hypothesize that this is due to a lower level of AM depletion caused by the PR8-PB1-F2(1918), which may be connected to the lower viral titer at 7d pii when the bacterial infection was initiated (Figure S3B inset). This is also in accordance with our model prediction that differences in bacterial dynamics were due to the antecedent viral infection<sup>17</sup>.

With only a short window where the surviving AMs are able to control bacterial growth, the opportunity for successful treatment while the immune system has the upper hand may be limited. Our results indicate that one preventative strategy (replenishment of AMs) and one therapeutic strategy (early reduction in bacterial loads), used separately or in combination, could be effective because the ratio of AMs to bacteria is the critical quantity that needs to be increased to abrogate secondary pneumococcal pneumonia. Reducing the transmitted dose is ideal, but this is difficult to control in practice. To prevent a coinfection, the AM population can be partially restored via immune modulators such as granulocyte macrophage colony stimulating factor (GM-CSF)<sup>18</sup>. In a study where mice were treated with recombinant GM-CSF (rGM-CSF) at -1d and 1d pii, the AM population increased by ~20% 2d after treatment (3d pii) and bacterial clearance in the first 3 h after inoculation at this time point improved by ~14%<sup>18</sup>. Further, pneumonia was reduced from 100% to 40% and 2 out of 10 of the treated mice were able to resolve the infection within 3 h compared to 0 in the untreated group. These results are consistent with those presented here, where a decrease in dose and thus an increase in the distance from the threshold results in faster clearance and resolution in some mice. Thus, similar outcomes will manifest through therapeutically decreasing AM depletion or decreasing bacterial loads, however the therapeutic requirement may change because of the nonlinearity of the relationship<sup>28</sup>. A more effective therapeutic approach may be to use antibiotics, which limit bacterial replication, either prophylactically or as an early treatment together with rGM-CSF<sup>28</sup>.

The importance of the AM:bacteria ratio suggests that the bacterial dose should be chosen carefully when designing pneumococcal or influenza-pneumococcal infection experiments so that misinterpretation of the results is avoided. For example, if a particular mouse strain has a greater number of AMs at baseline, a larger dose would be needed to examine a pneumococcal infection because a lower dose would be immediately cleared and the animal could be falsely regarded as protected. Further, sampling time should also be selected cautiously as important dynamics early in infection may be missed. However, based on our results, comparing the bacterial inoculum size to the final size and/or examining the heterogeneity in titers as we did here will help clarify where the experimental conditions are located along the AM:bacteria plane (Fig. 2A).

Until recently, it was unknown why the morbidity and mortality from influenza-pneumococcal coinfection is maximal at 7d pii<sup>19</sup>. Connecting the strength of bacterial growth to the depletion of AMs, which is maximal at 7d pii, provides the key to understanding coinfection kinetics<sup>17,18</sup>. Our work here quantitatively couples bacterial dose to these components and demonstrates that at least two simultaneous events (ample depletion combined with sufficient dose) are necessary for a coinfection to establish. Because both AM depletion and the dose effect are dynamic and likely dependent on other factors (e.g., AM depletion changes with viral strain), the probability of both events coinciding may be low. While a different virus strain is unlikely to impact the relationship we

established between bacterial dose and AM depletion, particularly given that we found the relationship is consistent for other mechanisms of AM depletion (e.g., cell death via clodronate-liposomes (Fig. 5)), strain dependent AM depletion may help to explain why only a proportion of influenza-infected individuals experience complications from secondary bacterial infections and why coinfections are less prevalent during seasonal epidemics<sup>29</sup>, where infections tend to be less severe compared to pandemic strains and may result in less AM depletion. When seasonal strains are in circulation, transmission of highly concentrated small particles (<10 µm), which are thought to deposit bacteria more readily into the lower airways (reviewed in ref. 30), may be required. In contrast, less concentrated and/or larger particles may be sufficient to establish a bacterial infection with more virulent strains of IAV.

Extending our results to predict the time scale at which the pneumonia progresses, the intensity of pneumonia, and the probability of survival may be more complicated. Our mathematical model (Equations (2–6)) is able to predict bacterial titer kinetics for a coinfection 7d p.i. and for infectious doses above or close to the initial dose threshold in which rapid growth ensues immediately<sup>17</sup>. We interpret the close fit of the model to the data (Figure S2) to mean that additional clearance mechanisms (e.g., neutrophils), which are currently excluded from the model, are ineffective. In the case where bacterial loads reach maximum levels (>10<sup>8</sup> CFU), mortality occurs in 100% of mice within 48–72 h p.i. The exact timing is dose-dependent and seems to be related to the rate at which this upper limit is achieved. However, predicting severity, outcome, and bacterial titers for infections with reduced doses, where bacterial titers may increase but remain low, is more challenging. We previously hypothesized that neutrophils may have a larger role in this context<sup>17</sup>. Understanding the inverse relationship between the rates of early clearance (0 → 4 h) and later growth (4 → 24 h) (Fig. 3B,C) does aid our ability to predict the resulting bacterial burden, but more complex and time-dependent dynamics, including inflammation and tissue damage, likely contribute to pathogenicity without significantly impacting bacterial loads.

Indeed, several other immune responses are elevated, dysfunctional, or otherwise altered during bacterial coinfection after influenza (reviewed in refs 7, 8, 9, 10, 11, 12, 13). For example, subsequent clearance mechanisms (>4 h p.i.), such as neutrophils and macrophages, undergo influenza-induced apoptosis, become dysfunctional, and have reduced chemotactic and phagocytic functions<sup>15,31–35</sup>. It is unclear the extent to which the inflated cytokine response (e.g., type I and II interferons (IFN-α, β, γ), TNF-α, IL-1β, IL-6, IL-12, and IL-10<sup>16,33,36–49</sup>) facilitates these changes. While our coinfection model does not explicitly account for these cytokines, the model's ability to accurately estimate AM loss with  $\hat{\phi}(V)$  indicates a limited role for cytokine-mediated functional inhibition of AMs. However, the cytokine response may be related to the observed viral rebound (Figure S2A), which our model suggests is independent of AM depletion and due to a bacterial induced increase in virus production/release ( $\hat{a}(P)$ )<sup>17</sup>. The increase in virus may be facilitated by the inhibition of IFN<sup>50</sup> resulting from bacterial adherence to virus-infected cells<sup>15,50,51</sup>. With the resulting heightened state of inflammation and severe lung damage, determining how each of these events is interrelated, dose-dependent, and connected to AM depletion is critical to finding new therapeutic approaches.

Analyzing coinfection kinetics with a mathematical model provides a means to quantify and simultaneously assess multiple infection characteristics. This method allows us to make meaningful predictions about the processes altered by each pathogen, even when exact mechanisms are unknown. It also permits *in silico* experiments for systems where data is difficult to obtain (e.g., in humans), and aids experimental design to test specific predictions. Carrying out targeted experimental studies based on analytical results, as done previously<sup>18,50</sup> and here, provides new biological insight about the underlying mechanisms and pinpoints improvements that can be made to our analysis. It is only with these improvements that we will be able to further examine the interactions between influenza, pneumococcus, and the host with new models that assess other immune components. Determining the circumstances that lead to severe bacterial infections during influenza and quantifying in detail how epidemiological factors (e.g., transmission dose) and host immune status (e.g., AM depletion) work together provides important clinical insight into the threat these pathogens pose to public health. Further establishing how other pathogen (e.g., strain, viral dose) and host (e.g., neutrophils, cytokines) factors are related and contribute to other infection characteristics (e.g., probability of pneumonia and disease progression/severity) will aid the development of therapies that prevent or treat these diseases.

## Methods

**Use of Experimental Animals.** All experimental procedures were approved by the Animal Care and Use Committee at SJCRH under relevant institutional and American Veterinary Medical Association guidelines and were performed in a Biosafety level 2 facility that is accredited by AALAAS.

**Influenza-Pneumococcal Coinfection Model.** We previously developed a model to describe influenza-pneumococcal coinfection kinetics<sup>17</sup>. Briefly, the model couples single infection models for influenza virus<sup>52</sup> and pneumococcus<sup>20</sup> and includes terms that describe their interactions<sup>17</sup>. Five populations are tracked: susceptible epithelial (“target”) cells ( $T$ ), two classes of infected cells ( $I_1$  and  $I_2$ ), virus ( $V$ ), and bacteria ( $P$ ).

$$\frac{dT}{dt} = -\beta TV \quad (2)$$

$$\frac{dI_1}{dt} = \beta TV - kI_1 - \mu PI_1 \quad (3)$$

$$\frac{dI_2}{dt} = kI_1 - \delta I_2 - \mu P I_2 \quad (4)$$

$$\frac{dV}{dt} = pI_2(1 + \hat{a}(P)) - cV \quad (5)$$

$$\frac{dP}{dt} = rP \left( 1 - \frac{P}{K_p(1 + \psi V)} \right) - \gamma_{M_A} f(P, M_A^*) M_A^* P (1 - \hat{\phi}(V)) \quad (6)$$

Target cells become infected with virus at rate  $\beta V$  per cell. Once infected, these cells enter an eclipse phase ( $I_1$ ) at rate  $k$  per cell before transitioning to produce virus at rate  $p$  per cell ( $I_2$ ). Virus is cleared at rate  $c$  and virus-producing infected cells ( $I_2$ ) are cleared at rate  $\delta$ . Bacteria replicate logistically with maximum rate  $r$  and tissue carrying capacity of  $K_p$ . Alveolar macrophages ( $M_A$ ) phagocytose bacteria at rate  $\gamma_{M_A} f(P, M_A)$  per cell. This rate decreases as the number of pneumococci increase according to  $f(P, M_A) = n^2 M_A / (P^2 + n^2 M_A)$ , where each AM is only able to phagocytose a maximum of  $n$  bacteria. Virus further decreases this clearance rate according to  $\hat{\phi}(V) = \phi V / (K_{pV} + V)$ . This term was shown to be the driving mechanism facilitating bacterial invasion<sup>17</sup> and matches the percentage of AM depletion<sup>18</sup>. Once bacteria invade, virus production/release from infected epithelial cells ( $pI_2$ ) is increased by a factor of  $\hat{a}(P) = aP^z$ . This term was shown to be the driving mechanism resulting in a viral rebound<sup>17</sup> and may result from IFN inhibition as a consequence of bacterial attachment to infected cells<sup>17,50</sup>. The model also assumes that virus infection increases the tissue carrying capacity ( $\psi V$ ), which may facilitate bacterial adhesion to cells, and that bacteria increase infected cell death ( $\mu P$ ). However, these two effects were shown to have minimal influence on the dynamics<sup>17</sup>. Altering other processes in the model, such as the rates of viral infection ( $\beta V$ ) and clearance ( $c$ ), produced minimal effects on model dynamics. The model schematic is shown in Figure S1, the model fits to lung viral and bacterial titers from groups of mice infected 7d after influenza A/Puerto Rico/8/34 (H1N1) (PR8) with PBS or pneumococcal strain D39 are shown in Figure S2, and the model parameters are in Table S1<sup>17</sup>.

**Derivation of the Initial Dose Threshold.** We used standard steady state and bifurcation analyses on the coinfection model to derive the initial dose threshold. Setting Equations (2–6) equal to zero and solving yields 4 equilibria: a disease-free state (0, 0, 0, 0, 0) and three states with non-zero bacterial levels (0, 0, 0, 0,  $P^*$ ). The non-zero  $P^*$  values satisfy  $P^3 + BP^2 + CP + D = 0$  and are defined by

$$\begin{aligned} P_2^* &= M_1 + M_2 - \frac{B}{3} \\ P_{3,4}^* &= -\frac{1}{2}(M_1 + M_2) \mp \frac{\sqrt{3}}{2}(M_1 - M_2)i - \frac{B}{3} \end{aligned} \quad (7)$$

where

$$\begin{aligned} M_{1,2} &= \sqrt[3]{-\frac{q}{2} \pm \sqrt{\frac{u^3}{27} + \frac{q^2}{4}}} \\ u &= C - \frac{B^2}{3} \\ q &= D + \frac{2B^3 - 9BC}{27} \\ B &= -K_p \\ C &= n^2 M_A \\ D &= n^2 M_A K_p \left( \frac{\gamma_{M_A} M_A}{r} - 1 \right) \end{aligned}$$

For the parameter values in Table S1, three real solutions exist because  $\frac{\gamma_{M_A} M_A}{r} > 1$  and the discriminant,  $\Delta = B^2 C^2 - 4B^3 D - 4C^3 + 18BCD - 27D^2$ , is positive. One of the equilibria ( $P_4^*$ ) is excluded because it is negative and not biologically relevant. Both  $P_1^* = 0$  CFU and  $P_2^* = K_p$  CFU are stable while  $P_3^* = 9993.5$  CFU is unstable. The unstable state ( $P_3^*$ ) indicates a threshold such that bacterial growth reaches the maximum carrying capacity when  $P(t) > P_3^*$ , while clearance occurs for  $P(t) < P_3^*$ . Because  $V^* = 0$ , these equilibria are equivalent to those in the single infection models and  $P_3^* = 9993.5$  CFU corresponds to the initial dose threshold in the absence of an antecedent viral infection<sup>20</sup>.

However, virus is non-zero ( $V(t) > 0$ ) at the initiation of the bacterial infection and the model solution, which is influenced by changes in the coinfection parameters<sup>17</sup>, is then perturbed away from its steady state. Re-solving for the equilibria yields non-zero state defined by Equation (7) but with



$$D_{\phi} = n^2 M_A K_P \left( \frac{\gamma_{M_A} M_A}{r} (1 - \hat{\phi}) - 1 \right). \quad (8)$$

The two stable states remain unchanged ( $P_1^* = 0$  CFU and  $P_2^* = K_P$  CFU). The unstable, positive root,  $P_{3\phi}^*$ , is dependent on  $\hat{\phi}$  and real if  $\frac{\gamma_{M_A} M_A}{r} (1 - \hat{\phi}) > 1$  (i.e.,  $D_{\phi} > 0$ ). However, the root turns complex when  $\frac{\gamma_{M_A} M_A}{r} (1 - \hat{\phi}) < 1$  (i.e.,  $D_{\phi} < 0$ ). The point where  $P_{3\phi}^*$  switches from being a real root to a complex root with real part less than 1 is found by solving  $D_{\phi} = 0$  for  $\hat{\phi}$ , which gives the critical value in Equation (1). The equilibria are plotted against  $\hat{\phi}$  in Fig. 2A.

**Mice.** Adult (6 week old) female BALB/c mice were obtained from Jackson Laboratories (Bar Harbor, ME). Mice were housed in groups of 5 in high-temperature 31.2 cm × 23.5 cm × 15.2 cm polycarbonate cages with isolator lids. Rooms used for housing mice were maintained on a 12:12-hour light:dark cycle at 22 ± 2 °C with 50% humidity in the biosafety level 2 facility at St. Jude Children's Research Hospital (Memphis, TN). Prior to inclusion in the experiments, mice were allowed at least 7 days to acclimate to the animal facility such that they were 7 weeks old at the time of infection. Laboratory Autoclavable Rodent Diet (PMI Nutrition International, St. Louis, MO) and autoclaved water were available ad libitum. All experiments were performed under an approved protocol and in accordance with the guidelines set forth by the Animal Care and Use Committee at St. Jude Children's Research Hospital.

**Infectious Agents.** All experiments were done using the mouse adapted influenza A/Puerto Rico/8/34 (H1N1) (PR8) and type 2 pneumococcal strain D39 that was transformed with the lux operon (Xenogen) to make it bioluminescent<sup>33</sup>.

**Macrophage Depletion by Clodronate-Liposomes.** Clodronate-liposomes (5 mg/ml, clodronateliposomes.org) were delivered intranasally in 100 ul.

**Infection Experiments.** The viral infectious dose (TCID<sub>50</sub>) was determined by interpolation using the method of Reed and Muench<sup>54</sup> using serial dilutions of virus on Madin-Darby canine kidney (MDCK) cells. The bacterial infectious dose (CFU) was counted for serial dilutions of bacteria on tryptic soy-agar plates supplemented with 3% (vol/vol) sheep erythrocytes. Inocula were diluted in sterile PBS and administered intranasally to groups of 5 mice lightly anesthetized with 2.5% inhaled isoflurane (Baxter, Deerfield, IL) in a total volume of 100 ul (50 ul per nostril). Mice were inoculated with 50 TCID<sub>50</sub> PR8 at day 0 and with D39 at 1, 3, 5, 7, 9, or 11 d p.i. at the doses listed in Table 2. Clodronate-liposome treated mice were inoculated with either PBS or D39 at 4 h post-treatment at a dose of 1, 10, or 100 CFU in 100 ul. Mice were weighed at the onset of infection and each subsequent day for illness and mortality. Mice were euthanized if they became moribund or lost 30% of their starting body weight. We repeated each experiment at least one time to ensure reproducibility.

**Lung Titers.** Mice were euthanized by CO<sub>2</sub> asphyxiation. Lungs were aseptically harvested, washed three times in PBS, and placed in 500 ul PBS. Lungs were mechanically homogenized using the Ultra-Turrax T8 homogenizer (IKA-werke, Staufen, Germany). Lung homogenates were pelleted at 10,000 rpm for 5 minutes and the supernatants were used to determine the bacterial titer for each set of lungs using serial dilutions on tryptic soy-agar plates supplemented with 3% (vol/vol) sheep erythrocytes.

**Flow Cytometric Analysis of Alveolar Macrophages.** After euthanasia by CO<sub>2</sub> inhalation, whole lungs were harvested, digested with collagenase (1 mg/ml, Sigma C0130), and physically homogenized by syringe plunger against a 40 um cell strainer. Cell suspensions were centrifuged at 4 °C, 500 × g for 7 min. Following red blood cell lysis, cells were washed in MACS buffer (PBS, 0.1 M EDTA, 0.01 M HEPES, 5 mM EDTA and 5% heat-inactivated FBS) and counted with trypan blue exclusion using a Cell Countess System (Invitrogen, Grand Island, NY). Flow cytometry (LSRII Fortessa; Becton Dickinson, San Jose, CA) was performed on the cell pellets after incubation with 200 ul of 1:2 dilution of Fc block (human-γ globulin) on ice for 30 min, followed by surface marker staining with anti-mouse antibodies: CD11c (eFluor450, eBioscience), CD11b (Alexa700, BD Biosciences), Ly6G (PerCp-Cy5.5, Biolegend), Ly6C (APC, eBioscience), F4/80 (PE, eBioscience), CD3e (PE-Cy7, BD Biosciences), CD4 (PE-Cy5, BD Biosciences), CD8a (BV605, BD Biosciences), DX5 (APC-Cy7, Biolegend) and MHC-II (FITC, eBioscience). The data were analyzed using FlowJo 10.0.8 (Tree Star, Ashland, OR) where viable cells were gated from a forward scatter/side scatter plot and singlet inclusion (see Figure S4). Following neutrophil exclusion (Ly6G<sup>hi</sup>), AMs were gated as CD11c<sup>hi</sup>F4/80<sup>hi</sup>CD11b<sup>-</sup>. The absolute numbers of different cell types were calculated based on viable events analyzed by flow cytometry as related to the total number of viable cells per sample. We obtain the range of percentage of AMs depleted by normalizing the absolute number of AMs to the absolute number of AMs in a naive mouse (Fig. 5).

**Alveolar Macrophage Data.** The AM data in Fig. 2B is from ref. 18 (Copyright 2013. The American Association of Immunologists, Inc.). In brief, groups of five 6–8 week old female BALB/c mice were infected intranasally with the PR8 virus. Bronchoalveolar lavage fluid (BALF) was collected and whole lungs post-lavage were harvested. Cells were analyzed by flow cytometry and AMs were gated as Ly6G<sup>-</sup>F4/80<sup>hi</sup>CD11c<sup>hi</sup>CD11b<sup>-</sup>. Here, we use the AM data from the lung and obtain the percentage of AMs depleted by normalizing the absolute number of AMs at each time point to the average number of AMs in a naive mouse (Fig. 2B).

**Statistical Comparisons.** We used the statistical programming language R<sup>55</sup>. T-tests were used to determine significance of differences of bacterial titers. A  $p < 0.05$  was considered significant for these comparisons.

## References

- Thompson, W. *et al.* Influenza-associated hospitalizations in the United States. *JAMA-J. Am. Med. Assoc.* **292**, 1333–1340 (2004).
- Reed, C. *et al.* Estimating influenza disease burden from population-based surveillance data in the United States. *PLoS One* **10**, e0118369 (2015).
- Morens, D., Taubenberger, J. & Fauci, A. Predominant role of bacterial pneumonia as a cause of death in pandemic influenza: implications for pandemic influenza preparedness. *J. Infect. Dis.* **198**, 962–970 (2008).
- Chien, Y., Klugman, K. & Morens, D. Bacterial pathogens and death during the 1918 influenza pandemic. *New Engl. J. Med.* **361**, 2582–2583 (2009).
- Louria, D., Blumenfeld, H., Ellis, J., Kilbourne, E. & Rogers, D. Studies on influenza in the pandemic of 1957–1958. II. Pulmonary complications of influenza. *J. Clin. Invest.* **38**, 213–265 (1959).
- Weinberger, D. *et al.* Impact of the 2009 influenza pandemic on pneumococcal pneumonia hospitalizations in the United States. *J. Infect. Dis.* **205**, 458–465 (2012).
- McCullers, J. The co-pathogenesis of influenza viruses with bacteria in the lung. *Nat. Rev. Microbiol.* **12**, 252–262 (2014).
- Metzger, D. & Sun, K. Immune dysfunction and bacterial coinfections following influenza. *J. Immunol.* **191**, 2047–2052 (2013).
- Brundage, J. Interactions between influenza and bacterial respiratory pathogens: implications for pandemic preparedness. *Lancet Infect. Dis.* **6**, 303–312 (2006).
- Short, K., Habets, M., Hermans, P. & Diavatopoulos, D. Interactions between *Streptococcus pneumoniae* and influenza virus: a mutually beneficial relationship? *Future Microbiol.* **7**, 609–624 (2012).
- Smith, A. & McCullers, J. Secondary bacterial infections in influenza virus infection pathogenesis. In *Influenza Pathogenesis and Control-Volume I*, 327–356 (Springer, 2014).
- Rynda-Applé, A., Robinson, K. & Alcorn, J. Influenza and bacterial superinfection: Illuminating the immunologic mechanisms of disease. *Infect. Immun.* **83**, 3764–3770 (2015).
- Robinson, K., Kolls, J. & Alcorn, J. The immunology of influenza virus-associated bacterial pneumonia. *Curr. Opin. Immunol.* **34**, 59–67 (2015).
- El Ahmer, O., Raza, M., Ogilvie, M., Weir, D. & Blackwell, C. Binding of bacteria to HEp-2 cells infected with influenza A virus. *FEMS Immunol. Med. Microbiol.* **23**, 331–341 (1999).
- Peltola, V. & McCullers, J. Respiratory viruses predisposing to bacterial infections: role of neuraminidase. *Pediatr. Infect. Dis.* **23**, S87–S97 (2004).
- Sun, K. & Metzger, D. Inhibition of pulmonary antibacterial defense by interferon- $\gamma$  during recovery from influenza infection. *Nat. Med.* **14**, 558–564 (2008).
- Smith, A. *et al.* Kinetics of coinfection with influenza A virus and *Streptococcus pneumoniae*. *PLoS Pathog.* **9**, e1003238–e1003238 (2013).
- Ghoneim, H., Thomas, P. & McCullers, J. Depletion of alveolar macrophages during influenza infection facilitates bacterial superinfections. *J. Immunol.* **191**, 1250–1259 (2013).
- McCullers, J. & Rehg, J. Lethal synergism between influenza virus and *Streptococcus pneumoniae*: Characterization of a mouse model and the role of platelet-activating factor receptor. *J. Infect. Dis.* **186**, 341–350 (2002).
- Smith, A., McCullers, J. & Adler, F. Mathematical model of a three-stage innate immune response to a pneumococcal lung infection. *J. Theor. Biol.* **276**, 106–116 (2011).
- Camberlein, E. *et al.* Importance of bacterial replication and alveolar macrophage-independent clearance mechanisms during early lung infection with *Streptococcus pneumoniae*. *Infect. Immun.* **83**, 1181–1189 (2015).
- Clement, C. *et al.* Stimulation of lung innate immunity protects against lethal pneumococcal pneumonia in mice. *Am. J. Resp. Crit. Care* **177**, 1322–1330 (2008).
- Domnguez-Cherit, G. *et al.* Critically ill patients with 2009 influenza A (H1N1) in Mexico. *JAMA - J. Am. Med. Assoc.* **302**, 1880–1887 (2009).
- Jain, S. *et al.* Hospitalized patients with 2009 H1N1 influenza in the United States, April–June 2009. *New Engl. J. Med.* **361**, 1935–1944 (2009).
- Jain, S. *et al.* Community-acquired pneumonia requiring hospitalization among US adults. *New Engl. J. Med.* **373**, 415–427 (2015).
- Jain, S. *et al.* Community-acquired pneumonia requiring hospitalization among US children. *New Engl. J. Med.* **372**, 835–845 (2015).
- Thepen, T., Van Rooijen, N. & Kraal, G. Alveolar macrophage elimination *in vivo* is associated with an increase in pulmonary immune response in mice. *J. Exp. Med.* **170**, 499–509 (1989).
- Smith, A. M. Quantifying the therapeutic requirements and potential for combination therapy to prevent bacterial coinfection during influenza. *J. Pharmacokinet. Pharm.* 1–13, doi: 10.1007/s10928-016-9494-9 (2016).
- Dawood, F. *et al.* Complications and associated bacterial coinfections among children hospitalized with seasonal or pandemic influenza, United States, 2003–2010. *J. Infect. Dis.* **209**, 686–694 (2014).
- Fernstrom, A. & Goldblatt, M. Aerobiology and its role in the transmission of infectious diseases. *J. Pathog.* **2013** (2013).
- Colamussi, M., White, M., Crouch, E. & Hartshorn, K. Influenza A virus accelerates neutrophil apoptosis and markedly potentiates apoptotic effects of bacteria. *Blood* **93**, 2395–2403 (1999).
- McNamee, L. & Harmsen, A. Both influenza-induced neutrophil dysfunction and neutrophil-independent mechanisms contribute to increased susceptibility to a secondary *Streptococcus pneumoniae* infection. *Infect. Immun.* **74**, 6707–6721 (2006).
- Small, C. *et al.* Influenza infection leads to increased susceptibility to subsequent bacterial superinfection by impairing NK cell responses in the lung. *J. Immunol.* **184**, 2048–2056 (2010).
- Engelich, G., White, M. & Hartshorn, K. Neutrophil survival is markedly reduced by incubation with influenza virus and *Streptococcus pneumoniae*: role of respiratory burst. *J. Leukoc. Biol.* **69**, 50–56 (2001).
- Kobayashi, S. *et al.* Bacterial pathogens modulate an apoptosis differentiation program in human neutrophils. *P Natl Acad Sci USA* **100**, 10948–10953 (2003).
- Shahangian, A. *et al.* Type I IFNs mediate development of postinfluenza bacterial pneumonia in mice. *J. Clin. Invest.* **119**, 1910–1920 (2009).
- Conenello, G. *et al.* A single N66S mutation in the PB1-F2 protein of influenza A virus increases virulence by inhibiting the early interferon response *in vivo*. *J. Virol.* **85**, 652–662 (2011).
- Nakamura, S., Davis, K. & Weiser, J. Synergistic stimulation of type I interferons during influenza virus coinfection promotes *Streptococcus pneumoniae* colonization in mice. *J. Clin. Invest.* **121**, 3657–3665 (2011).
- Tian, X. *et al.* Poly I:C enhances susceptibility to secondary pulmonary infections by gram-positive bacteria. *PLoS One* **7** (2012).
- Li, W., Moltedo, B. & Moran, T. Type I interferon induction during influenza virus infection increases susceptibility to secondary *Streptococcus pneumoniae* infection by negative regulation of  $\gamma\delta$  T cells. *J. Virol.* **86**, 12304–12312 (2012).
- Kudva, A. *et al.* Influenza A inhibits Th17-mediated host defense against bacterial pneumonia in mice. *J. Immunol.* **186**, 1666–1674 (2011).

42. Didierlaurent, A. *et al.* Sustained desensitization to bacterial Toll-like receptor ligands after resolution of respiratory influenza infection. *J. Exp. Med.* **205**, 323–329 (2008).
43. Wu, Y. *et al.* Successive influenza virus infection and *Streptococcus pneumoniae* stimulation alter human dendritic cell function. *BMC Infect. Dis.* **11**, 201 (2011).
44. Kuri, T. *et al.* Influenza A virus-mediated priming enhances cytokine secretion by human dendritic cells infected with *Streptococcus pneumoniae*. *Cell. Microb.* **15**, 1385–1400 (2013).
45. McAuley, J. *et al.* Expression of the 1918 influenza A virus PB1-F2 enhances the pathogenesis of viral and secondary bacterial pneumonia. *Cell Host & Microbe* **2**, 240–249 (2007).
46. Shepardson, K., K. M. and Larson *et al.* Differential type I interferon signaling is a master regulator of susceptibility to post-influenza bacterial superinfection. *mBio* **7**, e00506–16 (2016).
47. van der Sluijs, K. *et al.* IL-10 is an important mediator of the enhanced susceptibility to pneumococcal pneumonia after influenza infection. *J. Immunol.* **172**, 7603–7609 (2004).
48. Lee, B. *et al.* Influenza-induced type I interferon enhances susceptibility to gram-negative and gram-positive bacterial pneumonia in mice. *Am. J. Physiol-Lung C.* **309**, L158–L167 (2015).
49. Barthelemy, A. *et al.* Influenza A virus-induced release of interleukin-10 inhibits the anti-microbial activities of invariant natural killer T cells during invasive pneumococcal superinfection. *Mucosal Immunol* (2016).
50. Warnking, K. *et al.* Super-infection with *Staphylococcus aureus* inhibits influenza virus-induced type I IFN signalling through impaired STAT1-STAT2 dimerization. *Cell. Microbiol.* **17**, 303–317 (2015).
51. Peltola, V., Murti, K. & McCullers, J. Influenza virus neuraminidase contributes to secondary bacterial pneumonia. *J. Infect. Dis.* **192**, 249–257 (2005).
52. Baccam, P., Beauchemin, C., Macken, C., Hayden, F. & Perelson, A. Kinetics of influenza A virus infection in humans. *J. Virol.* **80**, 7590–7599 (2006).
53. McCullers, J. & Bartmess, K. Role of neuraminidase in lethal synergism between influenza virus and *Streptococcus pneumoniae*. *J. Infect. Dis.* **187**, 1000–1009 (2003).
54. Reed, L. & Muench, H. A simple method of estimating fifty percent endpoints. *Am. J. Epidemiol.* **27**, 493–497 (1938).
55. R Development Core Team. *R: A Language and Environment for Statistical Computing*. R Foundation for Statistical Computing, Vienna, Austria. URL <http://www.R-project.org>. ISBN 3-900051-07-0 (2006).

## Acknowledgements

This work was supported by NIH grants AI100946 and AI125324 and by ALSAC. We thank Fred Adler, Jon McCullers, and Alan Perelson for their helpful comments.

## Author Contributions

A.M.S. conceived the concept, planned the experiments, and wrote the manuscript. A.M.S. and A.P.S. performed the experiments. A.M.S. analyzed the model and data.

## Additional Information

**Supplementary information** accompanies this paper at <http://www.nature.com/srep>

**Competing financial interests:** The authors declare no competing financial interests.

**How to cite this article:** Smith, A. M. and Smith, A. P. A Critical, Nonlinear Threshold Dictates Bacterial Invasion and Initial Kinetics During Influenza. *Sci. Rep.* **6**, 38703; doi: 10.1038/srep38703 (2016).

**Publisher's note:** Springer Nature remains neutral with regard to jurisdictional claims in published maps and institutional affiliations.



This work is licensed under a Creative Commons Attribution 4.0 International License. The images or other third party material in this article are included in the article's Creative Commons license, unless indicated otherwise in the credit line; if the material is not included under the Creative Commons license, users will need to obtain permission from the license holder to reproduce the material. To view a copy of this license, visit <http://creativecommons.org/licenses/by/4.0/>

© The Author(s) 2016